# Predictive Value of Intratumoral ^{99m}Tc-Macroaggregated Albumin Uptake in Patients with Colorectal Liver Metastases Scheduled for Radioembolization with ^{90}Y-Mircrospheres

Gerhard Ulrich*[1], Oliver Dudeck*[1], Christian Furth[1], Juri Ruf[1], Oliver S. Grosser[1], Daniela Adolf[2], Marvin Stiebler[1], Jens Ricke[1], and Holger Amthauer[1]

[1]Department of Radiology and Nuclear Medicine, University of Magdeburg, Magdeburg, Germany; and [2]Department of Biometrics and Medical Informatics, University of Magdeburg, Magdeburg, Germany

[90]Y radioembolization is a promising therapy for patients with primary and secondary liver malignancies. Pretherapeutic assessment consists of hepatic angiography and ^{99m}Tc-macroaggregated albumin (^{99m}Tc-MAA) perfusion scintigraphy to estimate the liver-to-lung shunt and exclude extrahepatic ^{99m}Tc-MAA deposition. However, the predictive value of intratumoral ^{99m}Tc-MAA uptake remains unclear. **Methods:** One hundred four patients with chemotherapy-refractory liver-dominant metastatic colorectal cancer were treated with ^{90}Y radioembolization between December 2006 and December 2010. All of the patients underwent angiographic assessment and perfusion scintigraphy with ^{99m}Tc-MAA before lobar ^{90}Y radioembolization. For inclusion, patients must have undergone pretherapeutic and follow-up MR imaging (6 wk and 3 mo after radioembolization, respectively). The degree of intratumoral ^{99m}Tc-MAA uptake was rated, and liver metastases were classified according to changes in tumor diameter on both an individual and a patient basis using Response Evaluation Criteria In Solid Tumors (RECIST) 1.1. Response at both time points, MAA uptake, and catheter position were then statistically analyzed in a linear and generalized linear mixed model at a significance level of 0.05 (P value). **Results:** Sixty-six patients with a total of 435 colorectal liver metastases (mean number of lesions ± SD, 6.6 ± 2.8; mean lesion size ± SD, 33.8 ± 21.2 mm; lesion size range, 10–154 mm) were included in this analysis. According to the patient-based analysis, 3 patients had partial response, 49 stable disease, and 6 progressive disease after 6 wk. After 3 mo, 5 patients showed partial response, 26 stable disease, and 17 progressive disease. There was no association of patient-based tumor response with overall ^{99m}Tc-MAA uptake ($P = 0.172$) or with catheter position ($P = 0.6456$). Furthermore, an interaction effect of ^{99m}Tc-MAA uptake and catheter position in relation to tumor response was not found ($P = 0.512$). Moreover, in lesion-based analysis according to RECIST 1.1 there was no association of tumor response with degree of ^{99m}Tc-MAA uptake, catheter position, or interaction of ^{99m}Tc-MAA uptake and catheter position ($P = 0.339$, $0.593$, and $0.658$, respectively). **Conclusion:** Response to ^{90}Y radioembolization was found to be independent of the degree of ^{99m}Tc-MAA uptake. Therefore, therapy should not be withheld from patients with colorectal liver metastases lacking intratumoral ^{99m}Tc-MAA accumulation.

**Key Words:** radioembolization; perfusion scintigraphy; SIRspheres; response prediction

**R**adioembolization with ^{90}Y is a promising catheter-based liver-directed modality approved by the Food and Drug Administration for the treatment of patients with hepatic metastases of colorectal carcinoma (*1–4*). For this interventional technique, ^{90}Y-embedded microspheres of glass or resin are infused directly into the hepatic arteries, where they become lodged within the tumor microvasculature and irradiate the tumor by β-emission (*5*).

Perfusion scintigraphy with ^{99m}Tc-labeled macroaggregated albumin (^{99m}Tc-MAA) is mandatory before ^{90}Y radioembolization to identify extrahepatic visceral sites of tracer accumulation despite previous prophylactic microcoil embolization of extrahepatic vessels and to estimate the liver-to-lung shunt (*5–8*). For perfusion scintigraphy, SPECT has proven superior over planar scintigraphy, especially for the identification and topographic assignment of extrahepatic nuclide accumulation, particularly when coregistered with morphologic cross-sectional imaging (*9–11*). ^{99m}Tc-MAA has a particle size (10–50 μm; average particle size, 35 μm) comparable to resin microspheres (30–40 μm) and has therefore been propagated to simulate the expected microsphere distribution during ^{90}Y radioembolization. However, contradictory results have been published concerning the suitability of ^{99m}Tc-MAA uptake to predict the response of hepatic tumors to hepatic artery infusion chemotherapy and ^{90}Y radioembolization (*12–16*).

Therefore, the aim of this study was to evaluate whether the pattern of intratumoral ^{99m}Tc-MAA uptake in colorectal

liver metastases was predictive for the response to $^{90}$Y radioembolization.

## MATERIALS AND METHODS

### Patients

Between December 2006 and December 2010, 104 patients (mean age ± SD, 60.9 ± 10.0 y; age range, 30–78 y) with extensive colorectal liver metastases were treated with $^{90}$Y radioembolization. All patients had not been suitable for resection and had no option for further systemic chemotherapy. This study was approved by the local Ethics Committee, and all patients gave written informed consent for their treatment as required. Before treatment, patients underwent contrast-enhanced thoracoabdominal CT MR imaging of the liver with hepatocyte-selective contrast medium for the assessment of tumoral and nontumoral liver volume, portal vein patency, and the presence of extrahepatic disease. All patients were assessed with digital substraction angiography including prophylactic microcoil embolization of extrahepatic vessels before administration of $^{99m}$Tc-MAA for perfusion scintigraphy. For inclusion in this analysis, patients must have undergone $^{90}$Y radioembolization with pretherapeutic MRI (not longer than 30 d) and follow-up MR imaging. Confluencing hepatic metastases and lesions smaller than 10 mm on baseline MR imaging were excluded. In addition, no more than 10 lesions per patient were evaluated. At our institute, $^{90}$Y radioembolization is routinely performed in 2 sessions as a sequential treatment beginning with the liver lobe with predominant tumor burden; thus, lesions identified on Bremsstrahlung tomography located outside the treatment area of Bremsstrahlung emission were also excluded.

### MR Imaging Protocol

All MR examinations were performed on a 1.5-T MR system (Gyroscan, Intera; Philips Medical Systems) using a SENSE body coil (Philips). Imaging was performed at baseline immediately before $^{90}$Y radioembolization and at 6 wk and 3 mo after $^{90}$Y radioembolization. Examinations were performed with the following parameters: unenhanced T1-weighted imaging (gradient echo; repetition time [TR], 211 ms; echo time [TE], 3.3 ms; field of view [FOV], 450 cm; matrix, 256 × 144; SENSE factor, 2; and section thickness, 8 mm), T2-weighted fast-spin-echo imaging (TR, 1,600 ms; TE, 100 ms; flip angle, 80°; FOV, 450 cm; matrix, 384 × 196; SENSE factor; 2; and section thickness, 8 mm), and breath-hold axial single-shot echo planar diffusion-weighted T2-weighted fast-spin-echo imaging (TR, 1,850 ms; TE, 68 ms; b factors, 0 and 500 s/mm$^2$; matrix, 112 × 111; FOV, 450 cm; section thickness, 8 mm; number of signal averages, 2; half scan factor, 0.608). Then, gadolinium ethoxybenzyl diethylenetriamine pentaacetic acid (0.1 mmol/kg body weight; Primovist [Schering]) was administered with an infusion rate of 1.5 mL/s, followed by a 30-mL saline flush. T1-weighted 3-dimensional fast-field-echo imaging sequences were acquired with the following parameters: TR, 3.9 ms; TE, 1.9 ms; α, 10°; FOV, 450 cm; matrix, 192 × 136; SENSE factor, 2; section thickness, 6 mm; and spectral adiabatic inversion recovery. For subsequent acquisitions, intervals allowing the patient's free breathing were placed between the arterial and portal venous phases (20 s) and portal venous and equilibrium phases (i.e., interstitial) (40 s), respectively. T1-weighted 3-dimensional fast-field-echo and T1-weighted fast-spin-echo images (TR, 131 ms; TE, 5 ms; α, 70°; FOV, 450 cm; matrix, 256 × 135; SENSE factor, 2; and section thickness, 8 mm) at the hepatocyteselective (delayed) phase were acquired 10 and 20 min after contrast material was administered.

### Angiography and $^{99m}$Tc-MAA Perfusion Scintigraphy

Angiography was performed to evaluate the vascular anatomy of the liver and to assess the vascularization of liver metastases before $^{90}$Y radioembolization. To avoid extrahepatic deposition of microspheres (e.g., to the gastrointestinal tract), all vessels of concern such as the gastroduodenal, right gastric, supraduodenal, falciform, and cystic artery were embolized before $^{99m}$Tc-MAA assessment. $^{99m}$Tc-MAA ($^{99m}$Tc-TechneScan LyoMAA; Covidien Deutschland GmbH, Neustadt a. d.) was injected nonselectively (artery of proper or common hepatic artery) as a single dose in 18 of 66 patients (27.3%) or in a selective way as a split dose in the remaining 48 of 66 patients (72.7%). In 40 of 48 patients, the $^{99m}$Tc-MAA was applied in the right and left hepatic arteries, in 3 of 48 in the right hepatic artery only, in 1 of 48 in the right and middle hepatic arteries, and in 1 of 48 in the middle and left hepatic arteries. Mean applied activity for all patients was 153.4 ± 32.1 MBq of $^{99m}$Tc-MAA. To avoid nonspecific tracer uptake in the abdomen due to free $^{99m}$Tc, 600 mg of perchlorate was administered orally before angiography.

In all patients subject to $^{99m}$Tc-MAA perfusion scintigraphy, planar whole-body images and SPECT images of the abdomen were acquired. Imaging was performed with a double-head SPECT γ-camera (e.cam 180°; Siemens Healthcare). Planar whole-body scintigraphy was performed with a 256 × 1,024 matrix at a scan speed of 10 cm/min. SPECT was performed within a 128 × 128 matrix with 64 projections over 360° angle (30 s/projection) at an energy window of 140 keV (15% window width). For all imaging, low-energy high-resolution collimators were used. Tomograms were reconstructed by a 2-dimensional ordered-subset expectation maximization algorithm (17) with 8 iterations and 4 subsets. Attenuation correction was performed using the method of Chang (18), with the attenuation coefficient for water (μ = 0.15 cm$^{-1}$). Subsequently, the manual rigid fusion of SPECT and MR images was performed using software (workstation: e.soft turbo; Siemens Medical Inc.) that included dedicated image-fusion (Fusion 7D; Mirada Medical).

### $^{90}$Y Radioembolization

$^{90}$Y radioembolization using resin microspheres (SIR-Spheres; Sirtex Medical Europe) was performed sequentially starting with the liver lobe showing the predominant tumor load. Treatment over the right hepatic artery was performed in 48 of 66 patients (72.7%), over the left hepatic artery in 6 of 66 (9.1%), over the right and middle hepatic arteries in 6 of 66 (9.1%), over the left and middle hepatic arteries in 1 of 66 (1.5%), and over segmental hepatic arteries in 5 of 66 (7.6%). Overall, in 41 of 66 patients (62.1%), $^{90}$Y was applied in the identical vessel as $^{99m}$Tc-MAA, whereas in the other 25 of 66 patients (37.9%) the position varied. The first treatment started 16.1 ± 11.0 d after $^{99m}$Tc-MAA perfusion scintigraphy. Mean activity of the first treatment session for all patients was 1,146.5 ± 225.4 MBq of $^{90}$Y.

### Bremsstrahlung Tomography

After $^{90}$Y radioembolization, the distribution of the resin microspheres was evaluated by Bremsstrahlung tomography in all patients. Images were recorded with the aforementioned double-head γ-camera equipped with medium-energy general collimators. SPECT was performed with 128 projections over a 360° angle (30 s/projection) using a 128 × 128 matrix. The energy window was chosen in accordance with the suggestions by Minarik et al. (19) in the energy range of 75 keV (20% window width) (20). Tomograms

were reconstructed by a 2-dimensional ordered subset expectation maximation algorithm (*17*) with 8 iterations and 4 subsets. Attenuation correction was performed using the method of Chang (*18*), with a μ of 0.185 cm$^{-1}$. In the case of metastases in both liver lobes, $^{90}$Y radioembolization of the contralateral lobe was performed after an interval of 4–6 wk.

## Image Analysis

Images were analyzed by an experienced radiologist and nuclear medicine physician each in a consensus reading. MR images were analyzed on a PACS workstation (Infinitt Co., Ltd.). Lesions suitable for analysis were depicted on baseline MR images. Fused images of Bremsstrahlung tomograms and MR images were used to confirm that the identified lesions were located within the area of $^{90}$Y accumulation. The analysis was performed with dedicated image-fusion software (Fusion 7D Software; Mirada Medical). Metastases were numbered by placing electronic labels to assess lesion size of baseline and follow-up MR images simultaneously. The intratumoral $^{99m}$Tc-MAA accumulation on fused MR images/$^{99m}$Tc-MAA SPECT images was classified into 4 groups (1, no intratumoral $^{99m}$Tc-MAA uptake; 2, minimal $^{99m}$Tc-MAA uptake with no signs of central necrosis on MR imaging; 3, profound $^{99m}$Tc-MAA uptake throughout the lesion or uptake at the tumor margins in lesions with central necrosis; and 4, strong $^{99m}$Tc-MAA uptake).

## Statistical Analysis

Statistical analysis was performed using the software SAS 9.2 (SAS Institute Inc.). The degree of $^{99m}$Tc-MAA uptake was classified as either low MAA (groups 1 and 2) or high MAA (groups 3 and 4). For patient-based analysis therapy, response of treated lesions was evaluated by Response Evaluation Criteria In Solid Tumors (RECIST) 1.1 (*21*). For lesion-based analysis, each lesion was analyzed according to RECIST 1.1. In addition, responding lesions (RLs), with a decrease in tumor diameter, and nonresponding lesions (NRLs), with an increase in tumor diameter, were categorized. For treatment response assessed with RECIST, a linear mixed model with 1 (concerning the follow-ups) or 2 (concerning the number of lesions per patient additionally) random effects was performed to evaluate the impact of $^{99m}$Tc-MAA uptake, catheter position of $^{99m}$Tc-MAA application, and their interaction on tumor response. For lesion-based analysis of changes in tumor size, a generalized linear mixed model with 2 random effects was applied. A $P$ value of 0.05 was set to be the level of statistical significance. All tests were performed at full nominal test level.

## RESULTS

Sixty-six of 104 patients (25 women, 41 men; mean age ± SD, 60 ± 10.3 y) with a total of 435 colorectal liver metastases (mean number of lesions ± SD, 6.6 ± 2.8; mean lesion size ± SD, 33.8 ± 21.2 mm; lesion size range, 10–154 mm) were included in this retrospective analysis. Thirty-eight patients had to be excluded from this analysis: in 18 patients, no follow-up MR image was available; 12 patients underwent pretherapeutic MR imaging more than 30 d before $^{90}$Y radioembolization; in 4 patients, metastases were not clearly distinguishable on follow-up MR imaging; in 2 patients, no hepatocyte-selective contrast medium was used for follow-up MR imaging; and in another 2 patients, SPECT data of perfusion scintigraphy were not available.

Of those 66 patients evaluated, the interval between initial MR imaging and $^{90}$Y radioembolization was 13.1 ± 8.4 d. Fifty-eight patients underwent follow-up MR imaging at 6 wk (43.8 ± 12.8 d) after therapy, 48 patients at 3 mo (94.7 ± 19.2 d) thereafter, and 41 patients underwent MR imaging at both time points.

In all patients, the liver-to-lung shunt was 6.6% ± 3.4%. Extrahepatic abdominal nuclide accumulation was found in 14 of 66 patients for perfusion scintigraphy, of which 6 patients required a reevaluation with angiography, additional coiling, and additional perfusion scintigraphy. In 8 patients, the causal vessel was identified retrospectively; thus, it was embolized at the time of $^{90}$Y radioembolization angiography or $^{90}$Y microspheres were given distally of the aberrant vessel.

## Lesion-Based Analysis According to Changes in Tumor Diameter

Four hundred thirty-five (mean lesion size ± SD, 33.9 ± 21.2 mm) colorectal liver metastases were identified at initial MR imaging, of which 377 lesions (58 patients) and 290 lesions (48 patients) could be analyzed at 6 wk and 3 mo, respectively. At the 6-wk follow-up examination, 211 (mean lesion size in baseline MR imaging ± SD, 33.4 ± 19.7 mm; decrease in diameter, −15.6% ± 15.1%) of 377 liver metastases were classified as RL, and 166 lesions (mean lesion size in baseline MR imaging ± SD, 35.8 ± 24.1 mm; increase in diameter, 26.1% ± 26.8%) were categorized as NRL. At 3 mo, 290 metastases were assessed; 144 (mean lesion size in baseline MR imaging ± SD, 32.7 ± 20.3 mm; decrease in diameter, −20.1% ± 16.9%) of the 290 were classified as RL and 146 (mean lesion size in baseline MR image ± SD, 30.3 ± 17.9 mm; increase in diameter, 39.8% ± 45.1%) as NRL (Fig. 1). Although no significant association between therapy [**Fig. 1**] response and degree of $^{99m}$Tc-MAA uptake was found, there was a tendency for an inverse correlation to yield better tumor response in low $^{99m}$Tc-MAA uptake ($P = 0.058$). There was no significant impact of catheter position ($P = 0.199$), and no interacting effect of $^{99m}$Tc-MAA uptake and catheter position on the therapy response was found ($P = 0.998$). Treatment response in relation to $^{99m}$Tc-MAA uptake and catheter position are summarized in Table 1. [**Table 1**]

## Lesion-Based Analysis According to RECIST 1.1

At 6 wk after $^{90}$Y radioembolization, tumor response in the treated liver lobe was rated as PR in 28 metastases (7.4%), as SD in 278 (73.7%), and as PD in 71 (18.8%). After 3 mo, 32 lesions (11.0%) were rated as PR, 164 (56.6%) as SD, and 94 as PD (32.4%). Again, no association of tumor response with the degree of $^{99m}$Tc-MAA uptake was found ($P = 0.339$). In addition, no association of therapy response in relation to catheter position ($P = 0.593$) and no interacting effect of $^{99m}$Tc-MAA uptake and catheter position on therapy response was found ($P = 0.658$). Treatment response in relation to $^{99m}$Tc-MAA uptake and to catheter position is summarized in Table 2. [**Table 2**]
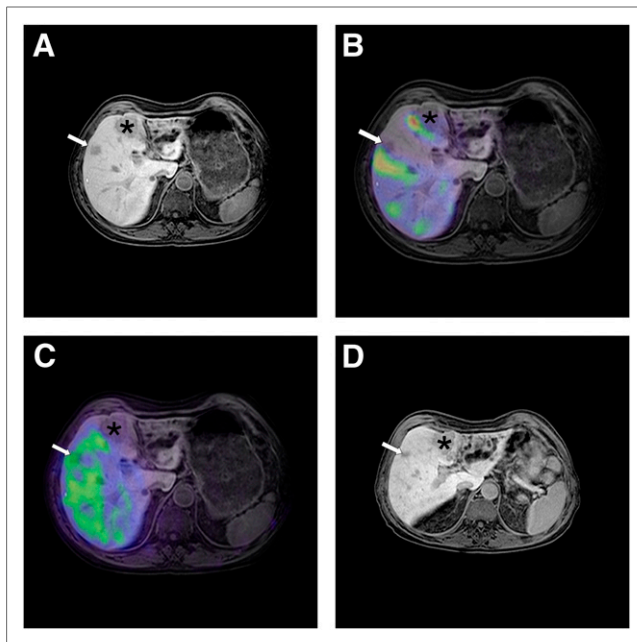
**FIGURE 1.** Sixty-six-year-old patient with hepatic metastases of colorectal carcinoma. Pretherapeutic contrast-enhanced MR imaging of liver (A) revealed in this axial slice intrahepatic lesion in segment 5 (arrow) and larger one in segment 4 (*). Perfusion scintigraphy using nonselective application of [99mTc]-MAA by proper hepatic artery (B) revealed heterogeneous intrahepatic distribution of administered nuclide without intratumoral accumulation in both hepatic metastases (B). After selective [90Y] radioembolization in right hepatic artery in sequential treatment plan, Bremsstrahlung scintigraphy was performed and fused with MR imaging. Pattern of [90Y]-labeled microspheres showed relatively homogeneous distribution in right liver lobe with accumulation in metastasis in segment 5 (arrow) and no accumulation in metastasis in segment 4 (*) (C). On follow-up MR image (D), 6 wk after [90Y] radioembolization there was clear decrease in size of treated metastasis in segment 5 (arrow) and stable situation of metastasis in segment 4 (*).

**RGB**

### Patient-Based Analysis

Three patients showed PR, 49 stable disease, and 6 PD after 6 wk. After 3 mo, 5 patients were classified as PR, 26 as SD, and 17 as PD. No association of tumor response with overall [99mTc]-MAA uptake was found at either follow-up interval ($P = 0.172$).

In addition, a possible influence of a change in catheter position at evaluation angiography, as compared with [90Y] application, was evaluated, but again no association of therapy response to the catheter position was found ($P = 0.646$). Furthermore, no interacting effect of [99mTc]-MAA uptake and catheter position on therapy response was observed ($P = 0.512$). Tables 3 and 4 show treatment response at 6 wk and 3 mo, respectively, in relation to patient age, [99mTc]-MAA activity, liver-to-lung shunt, [99mTc]-MAA uptake, delivered [90Y] activity, and catheter position. [Table 3] [Table 4]

### DISCUSSION

The results of this study demonstrate that the pattern of intratumoral [99mTc]-MAA uptake has no predictive value for the [90Y] radioembolization therapy response in patients with colorectal liver metastases. At first, this finding may come as a surprise because a locoregional transarterial treatment such as [90Y] radioembolization takes advantage of the aspect that liver metastases derive most of their blood supply from the hepatic artery whereas the hepatic parenchyma receives its supply predominantly from the portal vein (22). For transcatheter arterial chemoembolization as another locoregional transarterial treatment for patients with hypervascularized tumors such as hepatocellular carcinoma (HCC), it is well accepted that its success is highly dependent on the tumor vascularization, so that this treatment modality has become the standard of care in patients with intermediate-stage HCC (23). Consequently, it has been postulated that the mechanism of action for [90Y] radioembolization is flow-directed deposition of [90Y] microspheres

### TABLE 1
[99mTc]-MAA Uptake and Catheter Position in Relation to Lesion-Based Therapy Response

| Parameter | Tumor diameter after 6 wk (lesion total, $n = 377$) | | Tumor diameter after 3 mo (lesion total, $n = 290$) | |
|---|---|---|---|---|
| | RL ($n = 211$) | NRL ($n = 166$) | RL ($n = 144$) | NRL ($n = 146$) |
| [99mTc]-MAA uptake | | | | |
| Low | | | | |
| Group 1 | 53 (14.1) | 33 (8.8) | 29 (10.0) | 45 (15.5) |
| Group 2 | 48 (12.7) | 34 (9.0) | 32 (11.0) | 38 (13.1) |
| High MAA | | | | |
| Group 3 | 51 (13.5) | 66 (17.5) | 35 (12.1) | 49 (16.9) |
| Group 4 | 59 (15.6) | 33 (8.8) | 48 (16.6) | 14 (4.8) |
| Catheter position | | | | |
| Identical | 134 (35.5) | 115 (30.5) | 87 (30.0) | 100 (34.5) |
| Different | 77 (20.4) | 51 (13.5) | 57 (19.7) | 46 (15.9) |

Data in parentheses are percentages.

jnm112508-pm ■ 2/23/13

**TABLE 2**
$^{99m}$Tc-MAA Uptake and Catheter Position in Relation to Lesion-Based Therapy Response According to RECIST 1.1 After 6 Weeks and 3 Months

| | RECIST 1.1 after 6 wk (lesion total, $n = 377$) | | | RECIST 1.1 after 3 mo (lesion total, $n = 290$) | | |
|---|---|---|---|---|---|---|
| Parameter | PR ($n = 28$) | SD ($n = 278$) | PD ($n = 71$) | PR ($n = 32$) | SD ($n = 164$) | PD ($n = 94$) |
| $^{99m}$Tc-MAA uptake | | | | | | |
| Low | | | | | | |
|   Group 1 | 6 (1.6) | 65 (17.2) | 14 (3.7) | 2 (0.7) | 44 (15.2) | 28 (9.7) |
|   Group 2 | 4 (1.1) | 65 (17.2) | 14 (3.7) | 8 (2.8) | 36 (12.4) | 26 (9.0) |
| High | | | | | | |
|   Group 3 | 10 (2.7) | 72 (19.1) | 35 (9.3) | 9 (3.1) | 44 (15.2) | 31 (10.7) |
|   Group 4 | 8 (2.1) | 76 (20.2) | 8 (2.1) | 13 (4.5) | 40 (13.8) | 9 (3.1) |
| Catheter position | | | | | | |
|   Identical | 22 (5.8) | 176 (46.7) | 51 (13.5) | 22 (7.6) | 104 (35.9) | 61 (21.0) |
|   Different | 6 (1.6) | 102 (27.1) | 20 (5.3) | 10 (3.4) | 60 (20.7) | 33 (11.4) |

Data in parentheses are percentages.

into the vascular tumor bed and irradiation of the tumor by $\beta^-$ emissions of $^{90}$Y while the normal liver parenchyma is largely spared, thus combining the effects of interstitial high-dose radiotherapy and arterial microembolization (2,24). Nevertheless, the results of this study were obtained exclusively in patients with colorectal liver metastases, which can display various degrees of tumor vascularization and deposition of $^{99m}$Tc-MAA and $^{90}$Y microspheres (25).

Angiogenesis is a complex but fundamental requirement for tumor growth, invasion, and spread of metastases allowing newly formed metastatic nodules to rapidly coopt existing host vessels (26,27). Microvessel density analysis as an indicator of angiogenesis has been well described because it may resemble a prognostic factor and correlate with the aggressiveness and metastatic potential of solid tumors (28). Although it has been acknowledged that tumor vascularization of colorectal liver metastases is highly abnormal, a considerable heterogenity of the density of small tumor vessels at the liver-to-tumor interface (which represents the target area for $^{90}$Y microspheres) has been reported (28,29). Furthermore, the radiographic vascular appearance of liver metastases does not affect survival after $^{90}$Y radioembolization (30). Regarding the difference between the pattern of $^{99m}$Tc-MAA and $^{90}$Y microsphere deposition,

**TABLE 3**
Patient Demographics and Tumor Response Are Assessed by MR Imaging in Previously Treated Liver Lobe 6 Weeks After $^{90}$Y Radioembolization

| | RECIST 1.1 | | |
|---|---|---|---|
| Demographic | PR ($n = 3$) | Stable disease ($n = 49$) | PD ($n = 6$) |
| Age (y) | 65.7 ± 1.2 | 60.4 ± 11.0 | 59.5 ± 11.2 |
| Sex | | | |
|   Female ($n$) | 2 (3.4) | 19 (32.8) | 2 (3.4) |
|   Male ($n$) | 1 (1.7) | 30 (51.7) | 4 (6.9) |
| Dose of $^{99m}$Tc-MAA given (MBq) | 153.3 ± 7.6 | 152.4 ± 34.1 | 158.0 ± 32.3 |
| Liver-to-lung shunt (%) | 6.2 ± 4.5 | 6.6 ± 3.4 | 7.7 ± 3.7 |
| Dose of $^{90}$Y given (MBq) | 1,266.7 ± 208.2 | 1,144.6 ± 203.7 | 1,000.0 ± 298.3 |
| Low $^{99m}$Tc-MAA | | | |
|   Group 1 | 0 | 5 (8.6) | 0 |
|   Group 2 | 1 (1.7) | 17 (29.3) | 2 (3.4) |
| High $^{99m}$Tc-MAA | | | |
|   Group 3 | 1 (1.7) | 20 (34.5) | 3 (5.2) |
|   Group 4 | 1 (1.7) | 7 (12.1) | 1 (1.7) |
| Catheter position | | | |
|   Identical | 3 (5.2) | 30 (51.7) | 3 (5.2) |
|   Different | 0 | 19 (32.8) | 3 (5.2) |

Data are mean ± SD or $n$, with percentages in parentheses. Total number of patients was 58.

**TABLE 4**
Patient Demographics and Tumor Response Are Assessed by MR Imaging in Previously Treated Liver Lobe
3 Months After $^{90}$Y Radioembolization

| | RECIST 1.1 | | |
| --- | --- | --- | --- |
| Demographic | PR (n = 5) | Stable disease (n = 26) | PD (n = 17) |
| Age (y) | 59.6 ± 7.9 | 61.0 ± 12.5 | 58.8 ± 9.7 |
| Sex | | | |
|   Female (n) | 2 (4.2) | 10 (20.8) | 8 (16.7) |
|   Male (n) | 3 (6.3) | 16 (33.3) | 9 (18.8) |
| Dose of $^{99m}$Tc-MAA given (MBq) | 131.4 ± 31.1 | 152.6 ± 29.2 | 153.9 ± 30.9 |
| Liver-to-lung shunt (%) | 7.0 ± 2.4 | 5.9 ± 2.7 | 6.1 ± 2.4 |
| Dose of $^{90}$Y given (MBq) | 1,242.0 ± 181.2 | 1,179.2 ± 175.3 | 1,132.9 ± 278.3 |
| Low MAA | | | |
|   Group 1 | 0 | 4 (8.3) | 1 (2.1) |
|   Group 2 | 0 | 9 (18.8) | 9 (18.8) |
| High MAA | | | |
|   Group 3 | 3 (6.3) | 9 (18.8) | 4 (8.3) |
|   Group 4 | 2 (4.2) | 4 (8.3) | 3 (6.3) |
| Catheter position | | | |
|   Identical | 3 (6.3) | 14 (29.2) | 10 (20.8) |
|   Different | 2 (4.2) | 12 (25.0) | 7 (14.6) |

Data are mean ± SD or n, with percentages in parentheses. Total number of patients was 48.

several factors have to be addressed. Although the particles display almost similar sizes (10–50 μm for $^{99m}$Tc-MAA and 30–40 μm for resin microspheres), the number of particles infused is highly different. Although approximately 150,000 $^{99m}$Tc-MAA particles were infused for perfusion scintigraphy, the mean activity of a lobar liver dose of resin microspheres administered in this study was 1.14 GBq, which contains approximately 23 million microspheres (assuming an activity of 50 Bq per microsphere). As a result, the hepatic vasculature of the treated liver lobe is flooded with approximately 300 times more particles during $^{90}$Y radioembolization. Even in hypovascular lesions assessed as low MAA with $^{99m}$Tc-MAA, a sufficient amount of $^{90}$Y microspheres get lodged in the tumor microvasculature to induce relevant antitumor effects. Liver biopsies obtained from colon cancer metastases previously treated with resin microspheres showed an incongruent deposition, with the majority being located near tumor nodules. Although similar numbers of spheres were found at the tumor center and normal liver, the periphery of the tumor contained a 200-times greater concentration of spheres, with microspheres typically grouped in clusters of a few to several dozen spheres per cluster (31,32). In analyses of HCC patients who received resin microspheres, dose calculations based on measurements performed during laparotomy yielded doses between 34 and 1,474 Gy for tumor tissue whereas normal liver parenchyma received 9–75 Gy, resulting in a ratio of the number of microspheres seen in the tumor periphery, compared with nonneoplastic liver tissue (T:N ratio), of 0.4:1 up to 45:1 (33). A similar microsphere deposition can be observed in colorectal carcinoma although at a much lower level than in HCC, with T:N ratios ranging from 2:1 to 2:5 (24). Despite the obviously unavoidable deposition of

microspheres in regular liver tissue, an analysis by Ruehl et al. has shown that small amounts of microspheres in normal liver parenchyma are generally well tolerated, and radioembolization-induced liver disease occurs infrequently if $^{90}$Y radioembolization is performed as a sequential lobar treatment (34).

Obviously, no histologic data are available on the intrahepatic distribution pattern of $^{99m}$Tc-MAA; thus, the interpretation of the pattern is dependent on SPECT imaging. No relation could be found in our patients when the distribution pattern in both of the SPECT images and the corresponding lesional follow-up image were visually compared. This observation implies that in $^{99m}$Tc-MAA SPECT no prediction of response in colorectal carcinoma is possible. Therefore, pretherapeutic dosimetric calculations based on $^{99m}$Tc-MAA imaging, as reported for HCC (7,35), should be seen critically.

Taken together, according to our data it is not possible to predict the MR imaging–based therapy response from the degree of intratumoral $^{99m}$Tc-MAA uptake in perfusion scintigraphy. There is increasing evidence of a clinically relevant discrepancy of tumor response evaluation with metabolic $^{18}$F-FDG PET, as compared with traditional cross-sectional imaging (36). Recently, it has been shown that $^{18}$F-FDG PET can predict survival of breast cancer patients with hepatic metastases after $^{90}$Y radioembolization (37). In a small group of 8 patients with colorectal liver metastases who underwent $^{90}$Y radioembolization, the degree of $^{99m}$Tc-MAA uptake was found to correlate with the metabolic response as assessed with $^{18}$F-FDG PET (15). Unfortunately, $^{18}$F-FDG PET/CT is not routinely performed in patients scheduled for $^{90}$Y radioembolization at our

institute, so that we cannot contribute with additional data to these interesting findings.

## CONCLUSION

Our results demonstrate that in patients with colorectal liver metastases, therapy response after ^{90}Y radioembolization was independent of the degree of intratumoral ^{99m}Tc-MAA uptake. Consequently, therapy should not be withheld from patients with colorectal liver metastases lacking intratumoral ^{99m}Tc-MAA accumulation.

## DISCLOSURE

The costs of publication of this article were defrayed in part by the payment of page charges. Therefore, and solely to indicate this fact, this article is hereby marked "advertisement" in accordance with 18 USC section 1734. No potential conflict of interest relevant to this article was reported.

## REFERENCES

1. Geschwind JFH, Salem R, Carr BI, et al. Yttrium-90 microspheres for the treatment of hepatocellular carcinoma. *Gastroenterology*. 2004;127:S194–205.
2. Jakobs TF, Hoffmann R, Poepperl G, et al. Mid-term results in otherwise treatment refractory primary or secondary liver confined tumours treated with selective internal radiation therapy (SIRT) using [90]Yttrium resin-microspheres. *Eur Radiol*. 2007;17:1320–1330.
3. Sato KT, Lewandowski RJ, Mulcahy MF, et al. Unresectable chemorefractory liver metastases: radioembolization with ^{90}Y microspheres–safety, efficacy, and survival. *Radiology*. 2008;247:507–515.
4. Kennedy AS, Salem R. Radioembolization (yttrium-90 microspheres) for primary and metastatic hepatic malignancies. *Cancer J*. 2010;16:163–175.
5. Murthy R, Nunez R, Szklaruk J, et al. Yttrium-90 microsphere therapy for hepatic malignancy: devices, indications, technical considerations, and potential complications. *Radiographics*. 2005;25(suppl 1):S41–52.
6. Gray B, van Hazel G, Hope M, et al. Randomised trial of SIR-Spheres plus chemotherapy vs. chemotherapy alone for treating patients with liver metastases from primary large bowel cancer. *Ann Oncol*. 2001;12:1711–1720.
7. Ho S, Lau WY, Leung TW, et al. Partition model for estimating radiation doses from yttrium-90 microspheres in treating hepatic tumours. *Eur J Nucl Med*. 1996;23:947–952.
8. Lambert B, Mertens J, Sturm EJ, Stienaers S, Defreyne L, D'Asseler Y. ^{99m}Tc-labelled macroaggregated albumin (MAA) scintigraphy for planning treatment with ^{90}Y microspheres. *Eur J Nucl Med Mol Imaging*. 2010;37:2328–2333.
9. Hamami ME, Poeppel TD, Müller S, et al. SPECT/CT with ^{99m}Tc-MAA in radioembolization with ^{90}Y microspheres in patients with hepatocellular cancer. *J Nucl Med*. 2009;50:688–692.
10. Ahmadzadehfar H, Biersack H, Ezziddin S. Radioembolization of liver tumors with yttrium-90 microspheres. *Semin Nucl Med*. 2010;40:105–121.
11. Denecke T, Hildebrandt B, Lehmkuhl L, et al. Fusion imaging using a hybrid SPECT-CT camera improves port perfusion scintigraphy for control of hepatic arterial infusion of chemotherapy in colorectal cancer patients. *Eur J Nucl Med Mol Imaging*. 2005;32:1003–1010.
12. Daly JM, Butler J, Kemeny N, et al. Predicting tumor response in patients with colorectal hepatic metastases. *Ann Surg*. 1985;202:384–393.
13. Lehner B, Kretzschmar U, Bubeck B, Hölting T, Schlag P. Results of liver angiography and perfusion scintigraphy do not correlate with response to hepatic artery infusion chemotherapy. *J Surg Oncol*. 1988;39:73–78.
14. Civalleri D, Scopinaro G, Balletto N, et al. Changes in vascularity of liver tumours after hepatic arterial embolization with degradable starch microspheres. *Br J Surg*. 1989;76:699–703.
15. Flamen P, Vanderlinden B, Delatte P, et al. Multimodality imaging can predict the metabolic response of unresectable colorectal liver metastases to radioembolization therapy with yttrium-90 labeled resin microspheres. *Phys Med Biol*. 2008;53:6591–6603.
16. Dhabuwala A, Lamerton P, Stubbs RS. Relationship of 99mtechnetium labelled macroaggregated albumin (^{99m}Tc-MAA) uptake by colorectal liver metastases to response following selective internal radiation therapy (SIRT). *BMC Nucl Med*. 2005;5:7–16.
17. Hudson HM, Larkin RS. Accelerated image reconstruction using ordered subsets of projection data. *IEEE Trans Med Imaging*. 1994;13:601–609.
18. Chang LT. A method for attenuation correction in radionuclide computed tomography. *IEEE Trans Nucl Sci*. 1978;25:638–643.
19. Minarik D, Sjögreen Gleisner K, Ljungberg M. Evaluation of quantitative (90)Y SPECT based on experimental phantom studies. *Phys Med Biol*. 2008;53:5689–5703.
20. Grober OS, Nultsch M, Laatz K, et al. Radioembolization with (90)Y-labeled microspheres: post-therapeutic therapy validation with bremsstrahlung-SPECT. *Z Med Phys*. 2011;21:274–280.
21. Eisenhauer EA, Therasse P, Bogaerts J, et al. New response evaluation criteria in solid tumours: revised RECIST guideline (version 1.1). *Eur J Cancer*. 2009;45:228–247.
22. Breedis C, Young G. The blood supply of neoplasms in the liver. *Am J Pathol*. 1954;30:969–977.
23. Llovet JM, Real MI, Montaña X, et al. Arterial embolisation or chemoembolisation versus symptomatic treatment in patients with unresectable hepatocellular carcinoma: a randomised controlled trial. *Lancet*. 2002;359:1734–1739.
24. Kennedy AS, Nutting C, Coldwell D, Gaiser J, Drachenberg C. Pathologic response and microdosimetry of (90)Y microspheres in man: review of four explanted whole livers. *Int J Radiat Oncol Biol Phys*. 2004;60:1552–1563.
25. Dudeck O, Zeile M, Wybranski C, et al. Early prediction of anticancer effects with diffusion-weighted MR imaging in patients with colorectal liver metastases following selective internal radiotherapy. *Eur Radiol*. 2010;20:2699–2706.
26. Folkman J. How is blood vessel growth regulated in normal and neoplastic tissue? G.H.A. Clowes memorial Award lecture. *Cancer Res*. 1986;46:467–473.
27. Holash J, Maisonpierre PC, Compton D, et al. Vessel cooption, regression, and growth in tumors mediated by angiopoietins and VEGF. *Science*. 1999;284:1994–1998.
28. Rajaganeshan R, Prasad R, Guillou PJ, et al. The influence of invasive growth pattern and microvessel density on prognosis in colorectal cancer and colorectal liver metastases. *Br J Cancer*. 2007;96:1112–1117.
29. Mooteri S, Rubin D, Leurgans S, Jakate S, Drab E, Saclarides T. Tumor angiogenesis in primary and metastatic colorectal cancers. *Dis Colon Rectum*. 1996;39:1073–1080.
30. Sato KT, Omary RA, Takehana C, et al. The role of tumor vascularity in predicting survival after yttrium-90 radioembolization for liver metastases. *J Vasc Interv Radiol*. 2009;20:1564–1569.
31. Campbell AM, Bailey IH, Burton MA. Tumour dosimetry in human liver following hepatic yttrium-90 microsphere therapy. *Phys Med Biol*. 2001;46:487–498.
32. Campbell AM, Bailey IH, Burton MA. Analysis of the distribution of intra-arterial microspheres in human liver following hepatic yttrium-90 microsphere therapy. *Phys Med Biol*. 2000;45:1023–1033.
33. Burton MA, Gray BN, Klemp PF, Kelleher DK, Hardy N. Selective internal radiation therapy: distribution of radiation in the liver. *Eur J Cancer Clin Oncol*. 1989;25:1487–1491.
34. Rühl R, Seidensticker M, Peters N, et al. Hepatocellular carcinoma and liver cirrhosis: assessment of the liver function after Yttrium-90 radioembolization with resin 21 microspheres or after CT-guided high-dose-rate brachytherapy. *Dig Dis*. 2009;27:189–199.
35. Garin E, Lenoir L, Rolland Y, et al. Dosimetry based on 99m Tc-macroaggregated albumin SPECT/CT accurately predicts tumor response and survival in hepatocellular carcinoma patients treated with ^{90}Y-loaded glass microspheres: preliminary results. *J Nucl Med*. 2012;53:255–263.
36. Wong CYO, Salem R, Raman S, et al. Evaluating ^{90}Y-glass microsphere treatment response of unresectable colorectal liver metastases by CT or MRI. *Eur J Nucl Med Mol Imaging*. 2002;29:815–820.
37. Haug AR, Donfack BPT, Trumm C, et al. ^{18}F-FDG PET/CT predicts survival after radioembolization of hepatic metastases from breast cancer. *J Nucl Med*. 2012;53:371–377.